PHYSICAL REVIEW D **91,** 054039 (2015)

QCD radiation in *WH* and *WZ* production and anomalous coupling measurements

Francisco Campanario,[1,*] Robin Roth,[2,†] and Dieter Zeppenfeld[2,‡]

[1]*Theory Division, IFIC, University of Valencia-CSIC, E-46980 Paterna, Valencia, Spain*
[2]*Institute for Theoretical Physics, KIT, 76128 Karlsruhe, Germany*

(Received 6 November 2014; published 31 March 2015)

We study QCD radiation for the *WH* and *WZ* production processes at the LHC. We identify the regions sensitive to anomalous couplings, by considering jet observables, computed at next-to-leading-order QCD with the use of the Monte Carlo program VBFNLO. Based on these observations, we propose the use of a dynamical jet veto. The dynamical jet veto avoids the problem of large logarithms depending on the veto scale, hence providing more reliable predictions and simultaneously increasing the sensitivity to anomalous coupling searches, especially in the *WZ* production process.

DOI: 10.1103/PhysRevD.91.054039 PACS numbers: 12.38.Bx, 13.85.-t, 14.70.-e, 14.80.Bn

I. INTRODUCTION

Higgs production in association with a W boson is one of the main Higgs boson production mechanisms at the LHC. The LHC experiments did not yet observe the Higgs boson in this channel, but measurements are compatible with the Standard Model (SM) prediction [1,2]. This is also the case for the Tevatron CDF-D0 combination [3].

VH production is the best channel to measure the Higgs decay to $b\bar{b}$ at the LHC since the leptons from the V decay can be used for triggering and to reduce the backgrounds. Additionally, it allows the study of the VVH vertex and possible modifications to it by new physics entering via anomalous couplings (ACs). In this article, we will focus on WH production.

From the theoretical point of view, WH production has been extensively studied in the literature, and results at the next-next-to-leading order (NNLO) in QCD have been provided in Ref. [4] at the total cross section level and in Ref. [5] for differential distributions. Electroweak corrections to VH production including AC effects are available in HAWK [6]. AC effects are also a subject of interest [7].

Due to the large gluon luminosity, the fraction of WH events with additional jets is large. Results for WHj production at next-to-leading-order (NLO) are thus necessary, when one looks at one jet inclusive events as done by ATLAS [2]. Results for this process at NLO QCD have been reported both for W on-shell production [8] and also including the leptonic decays of the W [9].

In vector boson pair production processes, it is known that additional jet radiation reduces the sensitivity to AC measurements, results that have been confirmed at NLO in Refs. [10,11]. To reduce this effect and the sensitivity to higher QCD corrections, the traditional method has been to apply a jet veto above a fixed p_{T} [12], which comes with a naive reduction of scale dependence at the total cross section level. A closer look at the scale uncertainties in differential distributions reveals that exclusive samples inherit large scale uncertainties in the tails of the distributions, which are the regions most sensitive to AC effects. This has also been confirmed using merged samples for $WW(WZ)$ and $WWj(WZj)$ using the LOOPSIM method [13,14]. Thus, more sophisticated strategies in the current Monte Carlo driven analysis are needed to gain theoretical control.

In this paper, we study the jet radiation patterns at NLO QCD in WH and WZ production. We will show that they have distinctive signatures, and we will present a possible strategy to increase the sensitivity in those channels to AC searches. The constructed jet observables are shown at NLO QCD. To accomplish this, we have computed $WH(j)$ production at NLO QCD, including Higgs and leptonic W decays, and with the possibility to switch on AC effects. These processes are available in VBFNLO [15], a parton level Monte Carlo program which allows the definition of general acceptance cuts and distributions.

The paper is organized as follows. In Sec. II, the details of our calculation are given. Numerical results, including new strategies to enhance the sensitivity to AC searches will be given in Sec. III. Finally, in Sec. IV, we present our conclusions.

II. CALCULATIONAL SETUP

The WZ/WZj samples at NLO QCD are obtained from Refs. [16,17] available in the VBFNLO package [15]. The NLO QCD corrections to WZ production were first calculated in Ref. [18]. To compute the $WH(j)$ production processes at NLO QCD, we simplified the calculation for $l\nu_l\gamma\gamma j$ [19] production (from now on called $W\gamma\gamma j$ for simplicity) as explained below. For more details on the implementation and the checks performed, we refer the

*francisco.campanario@ific.uv.es
†robin.roth@kit.edu
‡dieter.zeppenfeld@kit.edu

reader to Ref. [20]. There, also, comparisons to earlier calculations of NLO QCD corrections to WHj production [8,9] are discussed. In the following, we sketch some details of our approach to make this work self-contained.

To compute the leading order (LO), virtual and real corrections, we use the effective current approach and the spinor-helicity amplitude method [21,22] factorizing the leptonic tensor containing the electroweak (EW) information of the system from the QCD amplitude. This allows us to obtain the code for the WHj process from the $W\gamma\gamma j$ code. For the $l\nu_l\gamma\gamma j$ process, first, the generic amplitudes $W\gamma\gamma j$, $\hat{W}\gamma j$ and $\tilde{W}j$ are created. Then, the leptonic decays $W \to l^+\nu$, $\hat{W} \to l^+\nu\gamma$ and $\tilde{W} \to l^+\nu\gamma\gamma$ are included via effective currents, incorporating, in this way, all off-shell effects and spin correlations of the process.

For obtaining the WHj amplitude, we select the generic $\tilde{W}j$ amplitude from the $W\gamma\gamma j$ process and use the appropriate leptonic current, i.e., $\tilde{W} \to l^+\nu H$. Decays of the Higgs boson factorize and can be included via branching ratios for the $H \to ff$ channels and via effective currents for the $H \to 4l$ ones. In this paper, an on-shell Higgs is assumed since off-shell effects contribute at the level of 10^{-3} and thus are negligible. For the WH process, we proceed in a similar way starting from $W\gamma$ production [16].

These changes are global in our code and have been cross-checked by comparing the LO and real emission corrections against Sherpa [23,24]. Agreement at the per mille level was found for integrated cross sections.

Quark mixing effects as well as the possibility to choose between the four-flavor and five-flavor scheme are available in the $WH(j)$ production process, but not for the $WZ(j)$ channel. Thus, for the sake of comparison, we use a unitary CKM matrix and work in the five-flavor scheme. Subprocesses with external top quarks are excluded since they are considered to be a different process, but virtual top-loop contributions are included in our calculation. They contribute at the few percent level at most.

Using the effective field theory formalism, the electroweak vertices such as the ones appearing in $WZ(j)$ and $WH(j)$ production can be extended to account for beyond the SM physics. These effects are constructed as additional terms in the Lagrangian with dimensionful couplings,

$$\mathcal{L} = \mathcal{L}_{\mathrm{SM}} + \sum_i \frac{f_i}{\Lambda^2}\mathcal{O}_i. \tag{1}$$

We use the basis presented in Refs. [25–27] to parametrize the AC. In our code, the anomalous trilinear couplings are included via purpose-built Helas routines which are again incorporated via effective currents; e.g., for $WH(j)$ production, we replaced $\tilde{W}$, by $\tilde{W} = \tilde{W}^{\mathrm{SM}} + \tilde{W}^{\mathrm{AC}}$, with $\tilde{W}^{\mathrm{SM}} \to l^+\nu H$ and $\tilde{W}^{\mathrm{AC}} \to l^+\nu H$, the latter via AC contributions coming from dimension-6 operators. The ones needed for the $WZ(j)$ production process were included in VBFNLO in a dedicated study in Ref. [10]. The specific ones for $WH(j)$ production were first included in Ref. [28].

While all relevant operators are implemented, we will focus the discussion on the operator

$$\mathcal{O}_W = (D_\mu\Phi)^\dagger \hat{W}^{\mu\nu}(D_\nu\Phi), \tag{2}$$

which does not only induce anomalous VVH couplings but also introduces modifications in WWV vertices and, thus, is severely constrained by LEP data already. The global fit of Ref. [29] bounds the coupling in the range $f_W/\Lambda^2 \in [-5.6, 9.6]$ TeV^{-2}, which is slightly more restrictive than the fit presented in Ref. [30].

In general, the AC contribution is most pronounced at large WH invariant mass. To measure AC effects, all contributing operators have to be considered, but we will focus and use $\mathcal{O}_W$ as a typical representative in the following. Note that there are remarkable differences in the coupling structure induced by $\mathcal{O}_W$ in the WWH and WWZ vertex.

To preserve tree level unitarity, we use a dipole form factor of the type

$$F = \left(1 + \frac{s}{\Lambda_{\mathrm{FF}}^2}\right)^{-p}, \tag{3}$$

with $p = 1$ and $\Lambda_{\mathrm{FF}} = 2$ TeV, where $\sqrt{s}$ denotes the WH or WZ invariant mass. The value for the form factor scale Λ_{FF} is derived from requiring that unitarity is preserved in $VV \to VV$ scattering using the form factor tool available on the VBFNLO website [31].

III. NUMERICAL RESULTS

In the following, we present results for the LHC operating at 14 TeV center-of-mass energy for the specific final states $e^+\nu_e H(j)$ and $e^+\nu_e\mu^+\mu^-(j)$ and refer to them respectively as $W^+H(j)$ and $W^+Z(j)$ production for simplicity. Results for $W^-H(j)$ and $W^-Z(j)$ production are very similar.

For input parameters, we use $M_W = 80.3980$ GeV, $M_Z = 91.1876$ GeV, $M_H = 126.0$ GeV and $G_F = 1.16637 \times 10^{-5}$ GeV^{-2} and derive the electromagnetic coupling constant and the weak-mixing angle from tree level relations. All the fermions are considered massless, except the top quark with $m_t = 172.4$ GeV. The resonating propagators are constructed with a constant width, fixed at $\Gamma_W = 2.098$ GeV, $\Gamma_Z = 2.508$ GeV and $\Gamma_H = 4.277$ MeV.

We use $\overline{MS}$ renormalization of the strong coupling constant α_s and the CTEQ CT10 NLO parton distribution functions [32] with $\alpha_s^{\mathrm{LO(NLO)}}(M_Z) = 0.1298(0.1180)$. The running of α_s includes five massless flavors, decoupling the top-quark contribution.

As a central value for the factorization and renormalization scale, we choose

$$\mu_0 = \frac{1}{2}\left(\sum_{\text{partons}} p_{T,i} + \sum_{W,Z/H}\sqrt{p_{T,i}^2 + m_i^2}\right), \qquad (4)$$

where m_i denotes the reconstructed invariant mass of the corresponding decay leptons or the on-shell boson. To give an estimate of the theoretical uncertainty, we show the scale dependence of the NLO cross section as bands in Figs. 4–6. There the factorization and renormalization scale are set to the same value varied simultaneously. The envelope of $\frac{1}{2}\mu_0$, μ_0 and $2\mu_0$, with μ_0 given from Eq. (4), is shown as a band labeled $2^{\pm 1}\mu_0$.

The jets are clustered using the anti-k_t algorithm [33] with a cone radius of $R = 0.4$. To simulate typical detector acceptance, we impose a minimal set of inclusive cuts,

$$\begin{aligned} &p_{\mathrm{T}l} > 20\ \text{GeV} \qquad p_{\mathrm{T}j} > 30\ \text{GeV} \qquad \not{p}_{\mathrm{T}} > 30\ \text{GeV} \\ &|\eta_j| < 4.5 \qquad |\eta_l| < 2.5 \qquad R_{l(l,j)} > 0.4 \\ &m_{ll} > 15\ \text{GeV} \qquad R_{ll} > 0.4, \end{aligned} \qquad (5)$$

where the m_{ll} cut is applied only to the leptons with opposite sign coming from the Z boson. To simulate VH experimental searches, we will also present results for boosted events requiring, additionally,

$$p_{\mathrm{T}Z/H} > 200\ \text{GeV}, \qquad (6)$$

where $p_{\mathrm{T}Z}$ is the reconstructed transverse momentum of the decay leptons.

The sensitivity to AC is not evenly distributed over phase space. A large contribution to the WZj cross section comes from events where the p_{T} of the Z boson and the leading jet balance and the W is soft, or similarly with W and Z exchanged. Those events can be considered as EW corrections to Vj production. Because the invariant mass of the electroweak system is small, they are less sensitive to AC effects. To suppress these events and also to reduce the impact of higher-order QCD corrections, a common approach is to apply a jet veto at fixed p_{T}. However, this procedure is problematic. The veto introduces terms of the form $\alpha_s^n \ln^{2n}(s/p_{\mathrm{T}j,\mathrm{veto}}^2)$, where s represents a typical scale of the hard process. For large values of s, this results in a poor control of our perturbative predictions, which may translate into large scale uncertainties of the observables. Note, however, that when studying inclusive samples the uncertainties are frequently underestimated by a naive scale variation. Such features have been extensively discussed for jet vetoes also in the context of NNLO calculations of Higgs-boson production; see, e.g., Refs. [34,35]. Instead of a fixed veto, of jets above a fixed transverse momentum, we will consider a specific dynamical veto in the following which avoids large logarithms by keeping the veto scale proportional to the hard scale of the process. For WV production, an effective dynamical jet veto has recently also been discussed in Ref. [36] in the context of observing large electroweak Sudakov logarithms at high transverse momenta.

In Tables I and II, we show the integrated cross sections for different jet multiplicities appearing at different orders of perturbation theory for the inclusive and the boosted set of cuts. We show cross sections for 8 and 14 TeV. Values for 13 TeV are 5% to 15% below the 14 TeV numbers.

One observes that a large fraction of the WZ production cross section is due to events with jets with $p_{Tj} > 30$ GeV. With boosted cuts, the NLO sample of WZj production has twice as many two-jet events as one-jet events. For WHj production, jet radiation is also significant. Thus, it is necessary to understand their radiation pattern and how to enhance regions sensitive to AC.

To visualize the phase space distributions of jets and weak bosons and their relative hardness, it is necessary to

TABLE I. Cross sections (in fb) for various jet multiplicities at LO and NLO for $e^+\nu_e\mu^+\mu^-(j)$ final states, for inclusive and boosted cuts as defined in Eqs. (5) and (6). The relative statistical error of the Monte Carlo integration is less than 3×10^{-3}.

	Inclusive				Boosted			
$\sqrt{s} = 8$ TeV	W^+Z		W^+Zj		W^+Z		W^+Zj	
N_{jets}	LO	NLO	LO	NLO	LO	NLO	LO	NLO
0	8.481	10.40			0.2145	0.1875		
1		4.841	4.867	4.195		0.3685	0.3730	0.2263
2				2.118				0.2712

	Inclusive				Boosted			
$\sqrt{s} = 14$ TeV	W^+Z		W^+Zj		W^+Z		W^+Zj	
N_{jets}	LO	NLO	LO	NLO	LO	NLO	LO	NLO
0	14.00	16.74			0.492	0.397		
1		11.28	11.31	8.391		1.242	1.248	0.554
2				6.223				1.094

TABLE II. Cross sections (in fb) for various jet multiplicities at LO and NLO for $e^+\nu_e H(j)$ final states, for inclusive and boosted cuts as defined in Eqs. (5) and (6). The relative statistical error of the Monte Carlo integration is less than 3×10^{-3}.

	Inclusive				Boosted			
$\sqrt{s} = 8$ TeV	W^+H		W^+Hj		W^+H		W^+Hj	
N_{jets}	LO	NLO	LO	NLO	LO	NLO	LO	NLO
0	24.85	24.81			1.716	1.467		
1		8.180	8.365	7.461		0.854	0.889	0.724
2				2.351				0.318
	Inclusive				Boosted			
$\sqrt{s} = 14$ TeV	W^+H		W^+Hj		W^+H		W^+Hj	
N_{jets}	LO	NLO	LO	NLO	LO	NLO	LO	NLO
0	47.08	44.12			4.103	3.188		
1		19.72	20.16	16.12		2.648	2.690	1.889
2				7.16				1.243

consider their transverse momenta in aggregate. In WVj events at LO, transverse momentum conservation implies $\mathbf{p}_{TW} + \mathbf{p}_{TV} + \mathbf{p}_{Tj} = 0$; i.e., there are four independent transverse momentum components. Discounting an overall rotation in the transverse plane and anticipating approximate invariance of radiation patterns under rescaling at very high energies, we are left with two parameters describing the essential features of the transverse motion and the relative importance of QCD radiation. These can be taken as the transverse energies of two of the three objects, normalized to the sum for all three; i.e., we consider

$$x_{\text{jet}} = \frac{\sum_{\text{jets}} \mathrm{E}_{\mathrm{T},i}}{\sum_{\text{jets}} \mathrm{E}_{\mathrm{T},i} + \sum_{W,Z/H} \mathrm{E}_{\mathrm{T},i}}, \tag{7}$$

and, similarly, for $V \in (W, Z, H)$ we define

$$x_V = \frac{E_{TV}}{\sum_{\text{jets}} \mathrm{E}_{\mathrm{T},i} + \sum_{W,Z/H} \mathrm{E}_{\mathrm{T},i}}. \tag{8}$$

Obviously, $x_{\text{jet}} + x_W + x_{Z/H} = 1$, and in a LO calculation, where a single massless parton forms the jet system which recoils against the other two objects, $x_{\text{jet}} < 0.5$.

A similar definition can be constructed using transverse momentum instead of transverse energy. However, in that case, x_{jet} is infrared sensitive and problematic in a fixed-order calculation, as will be discussed later.

A. x_{jet} vs $x_{Z/H}$ distributions

We can use these observables to draw a Dalitz-like 2D plot of $x_{\text{jet}}, x_{Z/H}$ where phase space regions with soft EW bosons can easily be distinguished from regions with soft jets. A value close to 0.5 for the $x_{\text{jet}(H,Z)}$ observable would indicate that the given particle has half of the total transverse energy of the system, recoiling against the rest, while values close to zero indicate that the particle is soft.

In Fig. 1, we show the LO double differential distributions for WZj and WHj production with respect to x_{jet} and $x_{Z/H}$ for inclusive (upper row) and boosted cuts (lower panels). On the left, WZj production is shown, and on the right, results for the WHj process are shown, replacing x_Z by the equivalent x_H observable.

Already the inclusive sample shows that WZj production allows for harder jets, while WHj production is dominated by back-to-back WH pairs with only soft jets. With the additional boosted cut, the difference is enhanced, and one can clearly observe the different radiation patterns of the WHj and WZj processes. While in WHj production soft QCD radiation is preferred, in the WZj case, there are two equally important phase space regions, those with soft jets at small x_{jet} and those with a soft W boson at large x_{jet}. The latter dilutes the sensitivity to AC of this process as will be shown below. The origin of these different radiation patterns is the partial wave decomposition of the WH/WZ final state. WH production is mostly restricted to $J = 1$, since it arises from a virtual W, while this is only a small contribution to WZ production.

Figure 2 shows the same distributions at NLO. There is an overall small shift to higher x_{jet} due to the presence of an additional parton in the real emission contributions. Still the jet dominated and EW dominated phase space regions can be clearly separated.

Note that the $x_{\text{jet}} = 0.5$ and $x_Z = 0.5$ borders show unphysical structures at NLO due to phase space restrictions of the 1-parton final states, which affect the Born and virtual corrections. In a final state with only one parton and thus exactly one massless jet after cuts, only $x_{\text{jet}} < 0.5$ is possible. With two or more partons, the x_{jet} definition allows values above 0.5, e.g., for two jets back-to-back with

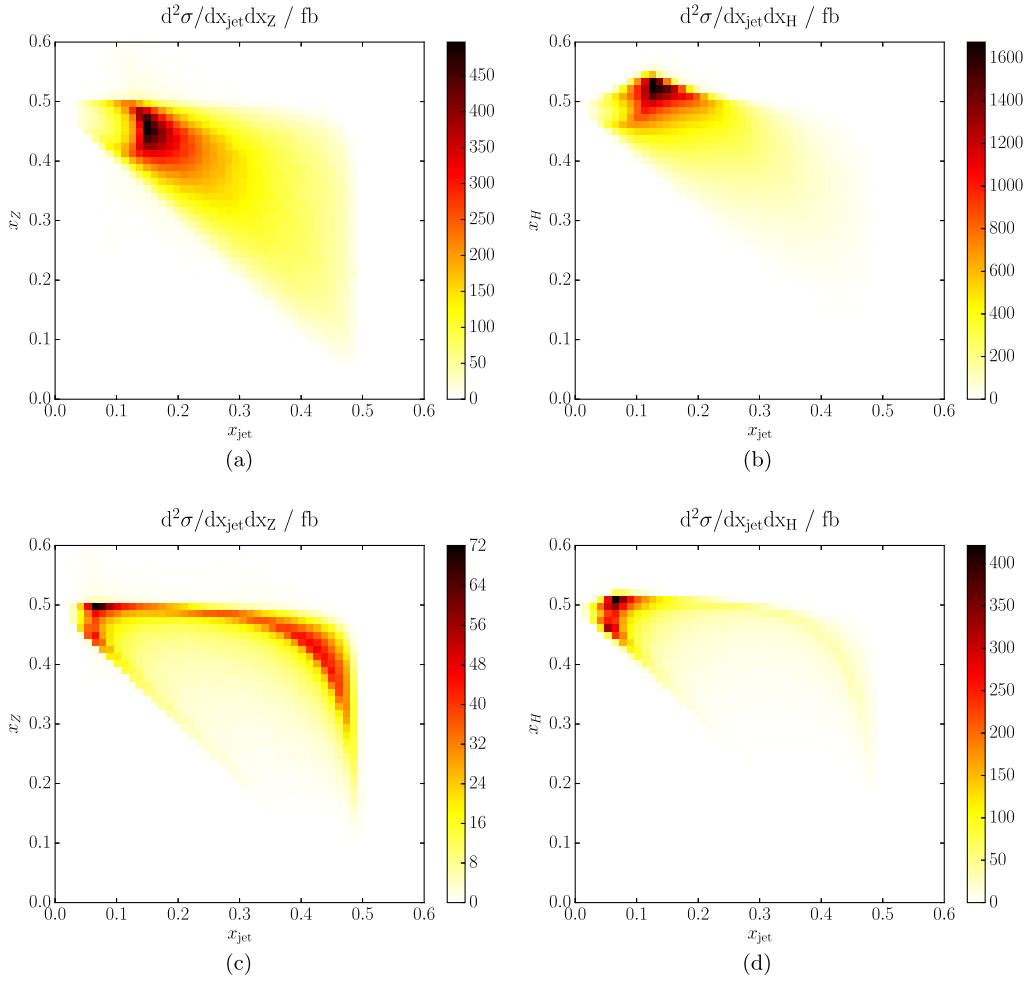

FIG. 1 (color online). LO double differential distributions for $e^+\nu_e\mu^+\mu^- j$ ($e^+\nu_e Hj$) production on the left (on the right) with respect to x_{jet} and x_Z (x_H). Inclusive cuts are used in the upper row, and boosted cuts ($p_{\text{T}H(Z)} > 200$ GeV) are in the bottom panels. (a) Inclusive W^+Zj. (b) Inclusive W^+Hj. (c) Boosted W^+Zj. (d) Boosted W^+Hj.

rather soft EW bosons or when there is a parton not clustered into the jets. Because this region is only available to the real emission at NLO and not to the subtraction terms or the virtual corrections, there is an unphysical negative dip just below 0.5. This problem affects an x_{jet} definition based on transverse momenta quite strongly, while the definition using E_T is safer since the masses act as a regulator. In Fig. 2, the dip is barely visible. A parton shower would completely wash out this artifact of the fixed-order calculation.

Well below $x_{\text{jet}} = 0.5$, these infrared issues are mitigated. In particular, the problem does not affect the region $x_{\text{jet}} < 0.2$, which is the region most sensitive to ACs, as is visible in Fig. 3, where we have used $f_W/\Lambda^2 = -10\ \text{TeV}^{-2}$ as an example. Note in the left panel of Fig. 3 that the relative importance of hard jet events, characteristic of the WZj process, has diminished considerably once ACs are turned on, highlighting the fact that AC effects are more prominent in back-to-back WZ topologies.

Figure 4 shows the one-dimensional projection of the differential x_{jet} distribution for different values of the AC. For small values of f_W/Λ^2, the dominant term is the interference between SM and AC contribution. Hence, their relative sign is important. For negative couplings there is constructive interference, while for positive values of the coupling, the interference is destructive. Thus, first the cross section decreases until the pure AC term outweighs the interference term, which happens for W^+Zj production at $f_W/\Lambda^2 \approx +10\ \text{TeV}^{-2}$. Both Figs. 3 and 4 show that the sensitivity to AC effects is in the low x_{jet} region, confirming that hard radiation dilutes the sensitivity to AC searches. We will impose a jet veto requiring $x_{\text{jet}} < 0.2$ to focus on the region most sensitive to AC. There is small sensitivity to AC up to about 0.3, such that this part of phase space should also be included in experimental searches.

A fixed scale jet veto typically introduces logarithms of the veto scale over the hard process scale. They are visible in form of a widening scale variation band for

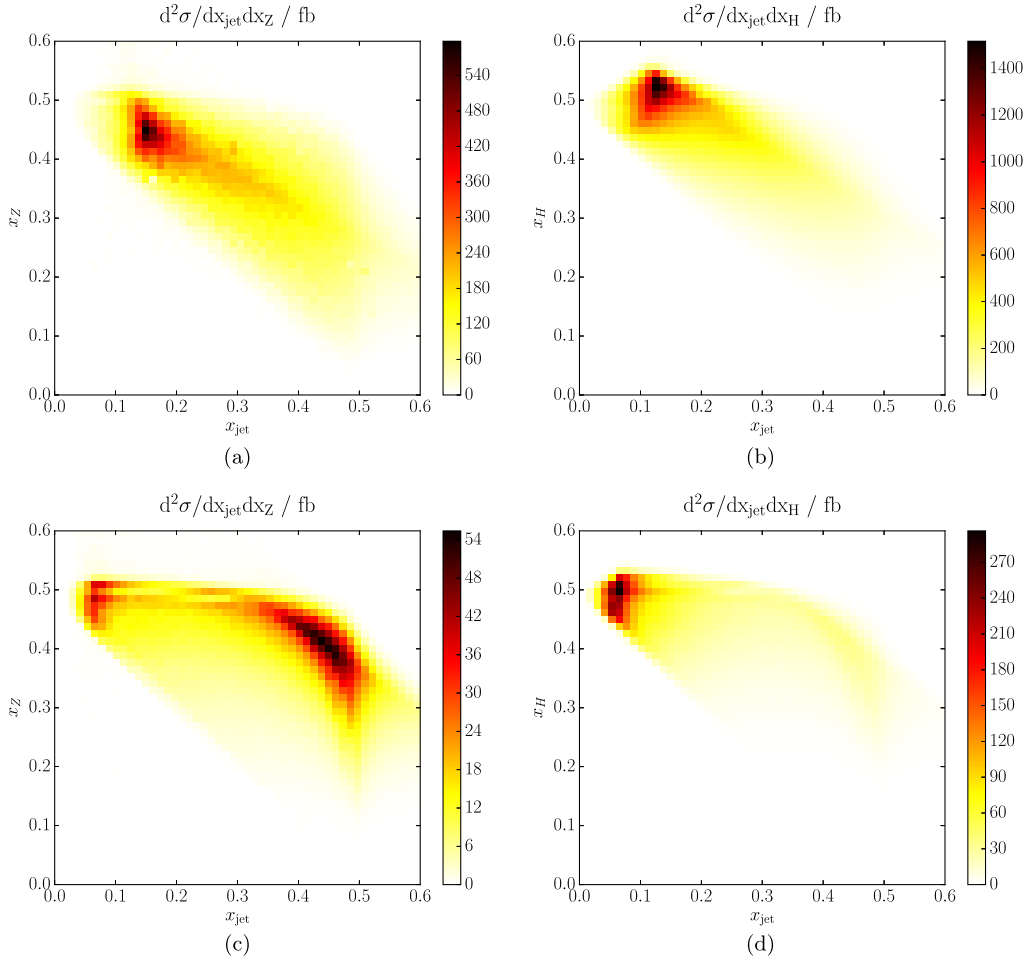

FIG. 2 (color online). Same as Fig. 1 but at NLO. (a) Inclusive W^+Zj. (b) Inclusive W^+Hj. (c) Boosted W^+Zj. (d) Boosted W^+Hj.

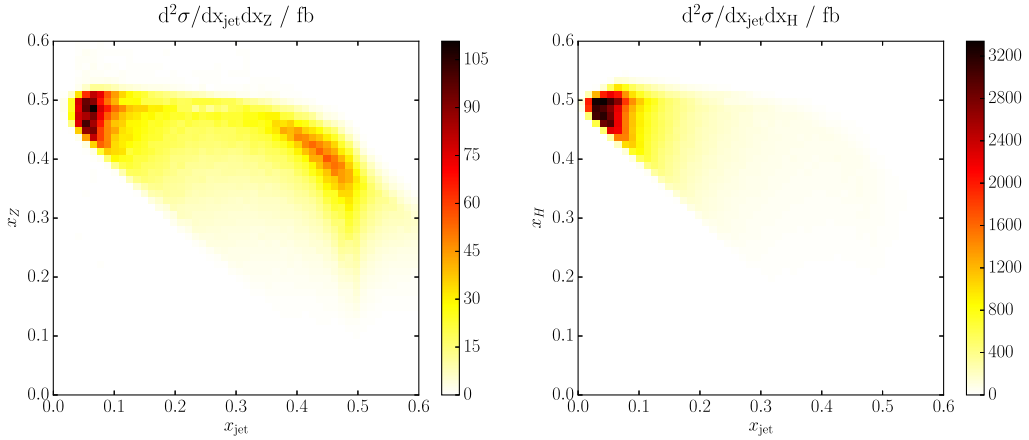

FIG. 3 (color online). Same as Fig. 1 but at NLO and with anomalous coupling effects switched on with $f_W/\Lambda^2 = -10$ TeV^{-2}. Results are shown for the boosted set of cuts for $e^+\nu_e\mu^+\mu^-j$ (left panel) and $e^+\nu_eHj$ production (right panel).

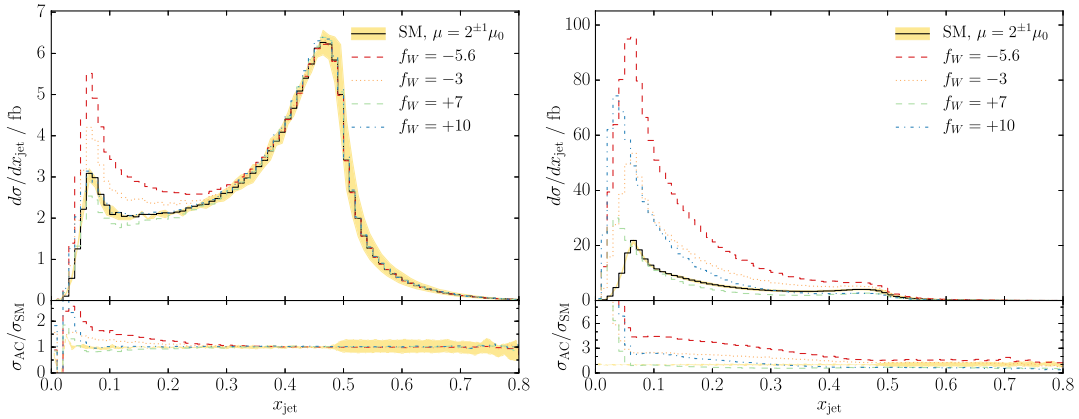

FIG. 4 (color online). $x_{\rm jet}$ distribution for $e^+\nu_e\mu^+\mu^- j$ (left) and $e^+\nu_e Hj$ (right) production for different values of AC with boosted cuts at NLO. The yellow band corresponds to the variation of $\mu = \mu_{\rm F} = \mu_{\rm R}$ by a factor of 2.

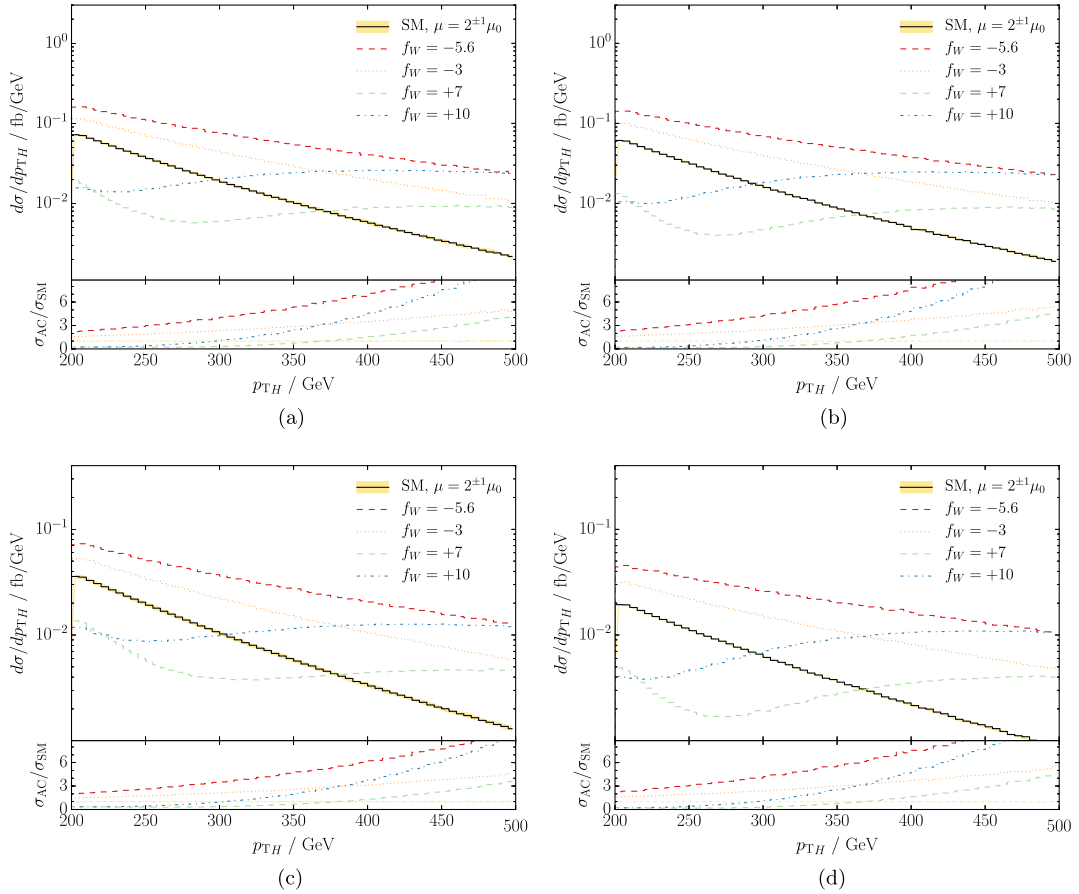

FIG. 5 (color online). Differential transverse momentum distribution of the H boson in $e^{\pm}\overset{(-)}{\nu}_e H(j)$ production for different values of the f_W parameter with (right) and without (left) a dynamical jet veto. The AC scale is chosen as $\Lambda = 1$ TeV. (a) $p_{{\rm T}H}$, W^+H, boosted. (b) $p_{{\rm T}H}$, W^+H, boosted, with jet veto. (c) $p_{{\rm T}H}$, W^+Hj, boosted. (d) $p_{{\rm T}H}$, W^+Hj, boosted, with jet veto.

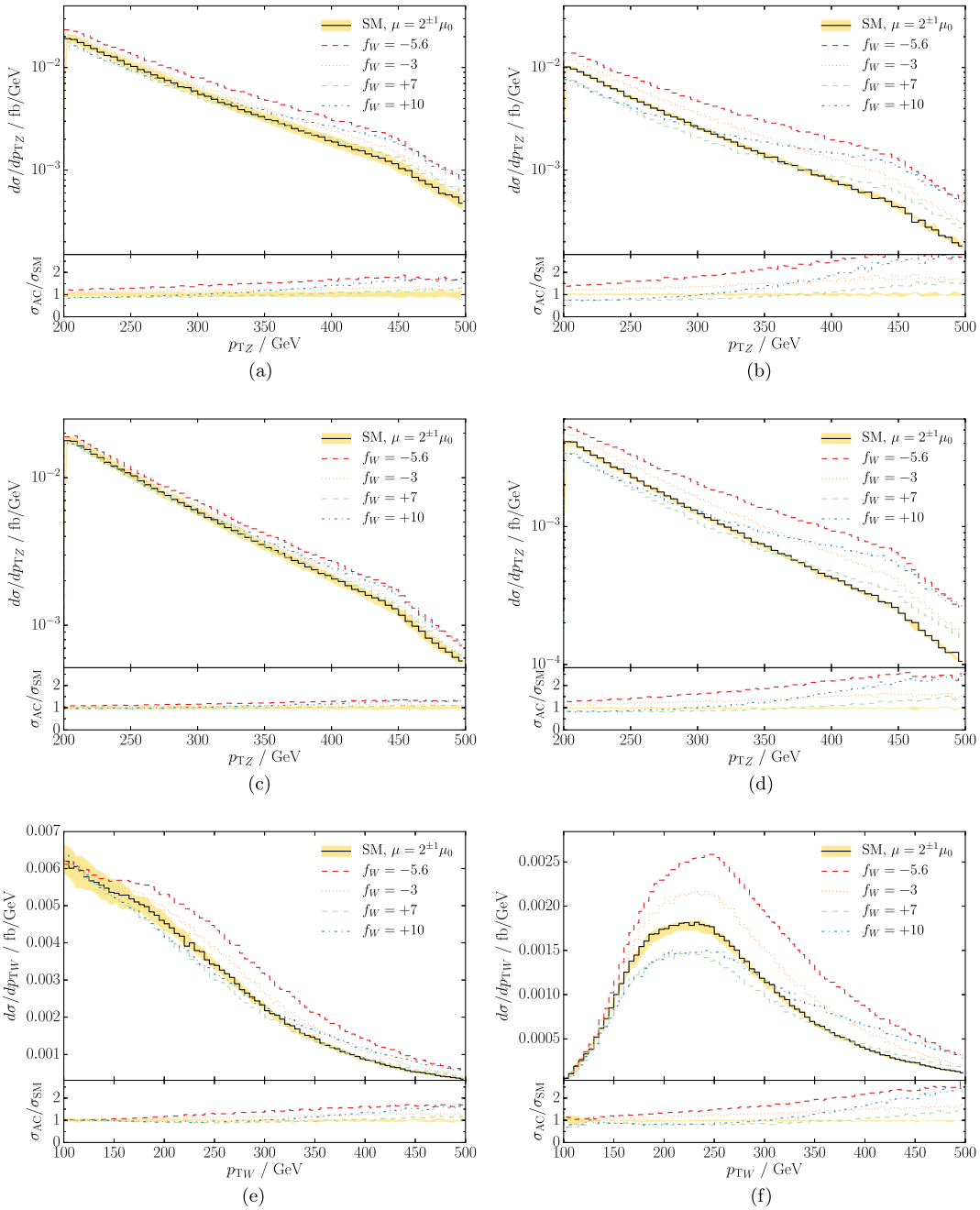

FIG. 6 (color online). Differential transverse momentum distribution of the reconstructed W and Z boson in $e^+\nu_e\mu^+\mu^-(j)$ production for different values of the f_W parameter with (right) and without (left) a dynamical jet veto. The AC scale is chosen as $\Lambda = 1$ TeV. (a) p_{Tz}, W^+Z, boosted. (b) p_{Tz}, W^+Z, boosted, with jet veto. (c) p_{Tz}, W^+Zj, boosted. (d) p_{Tz}, W^+Zj, boosted, with jet veto. (e) p_{TW}, W^+Zj, boosted. (f) p_{TW}, W^+Zj, boosted, with jet veto.

example in invariant mass or transverse momentum distributions as the energy increases. An indication, that the dynamical jet veto does result in more reliable theoretical predictions than a veto above a fixed jet transverse momentum, is that the scale variation bands of vetoed cross sections do not grow with energy but stay at a size comparable to the total boosted sample. Such scale variation bands are shown in Figs. 4–6.

B. Differential distributions

In Figs. 5 (6), we show transverse momentum differential distributions at NLO for $W^+H(j)$ ($W^+Z(j)$) production. WX production at NLO includes zero-jet and one-jet events, while WXj production at NLO requires at least one jet with $p_{Tj} > 30$ GeV.

In Fig. 5, we show the NLO differential distribution of the transverse momentum of the Higgs boson for the

boosted sample with (right) and without (left) applying the dynamical jet veto for W^+H production (upper panels) and for W^+Hj production (lower panels). The effect of AC is clearly visible in all distributions. As expected, there is only a mild improvement when applying the jet veto since there is little hard jet radiation in this process. The ratio $\sigma_{\mathrm{AC}}/\sigma_{\mathrm{SM}}$ improves from 4.0 to 5.0 due to the veto in case of $f_W = -5.6\ \mathrm{TeV}^{-2}$.

This situation needs to be contrasted with the case of WZ production, as shown in Fig. 6. In the upper panel, we consider the transverse momentum distribution of the Z boson for W^+Z production at NLO. Distributions are shown for the boosted sample with (right) and without (left) applying the dynamical jet veto. The effect of anomalous couplings is strongly enhanced by the jet veto, increasing $\sigma_{\mathrm{AC}}/\sigma_{\mathrm{SM}}$ from 1.36 to 1.72. Similarly, in the middle and lower rows, we show for W^+Zj production the differential distribution of the transverse momenta of the Z and the W bosons. Also here one can clearly see the improved AC sensitivity of the vetoed distributions. In the case of p_{TW}, the ratio $\sigma_{\mathrm{AC}}/\sigma_{\mathrm{SM}}$ increases from 1.3 to 1.5 at 250 GeV and from 1.7 to 2.8 at 500 GeV. For p_{TZ}, the increases at the same positions are from 1.1 to 1.5 and from 1.3 to 2.4, considering $f_W = -5.6\,\mathrm{TeV}^{-2}$.

IV. CONCLUSIONS

In this article, the QCD radiation patterns for the WZ and the WH production processes have been studied. To accomplished this, we have computed and implemented in VBFNLO the $WH(j)$ production process at NLO QCD, including the leptonic decay of the bosons as well as anomalous couplings effects.

Looking at jet observables, we find distinguishable radiation patterns comparing WH production with WZ production. While in $WH(j)$ production soft QCD radiation is preferred, in the $WZ(j)$ case with boosted cuts, there are two equally important phase space regions, those with soft jets and those with one hard vector boson recoiling against a jet and a second soft vector boson. The latter region dilutes the sensitivity of this process to AC. The two phase space regions can be separated quite cleanly by analyzing the Dalitz-like normalized transverse energy fractions defined in Eqs. (7) and (8).

To enhance the sensitivity to AC, a cut on the jet transverse energy fraction, x_{jet}, proves effective. At the same time, this dynamical jet veto provides more reliable results than a fixed veto because it avoids large logarithms involving the veto scale and thus has smaller scale variations.

ACKNOWLEDGMENTS

We would like to thank Johannes Bellm for helpful discussions and for the implementation of the WZ production process in VBFNLO. We acknowledge the support from the Deutsche Forschungsgemeinschaft via the Sonderforschungsbereich/Transregio SFB/TR-9 Computational Particle Physics. F. C. is funded by a Marie Curie fellowship (Grant No. PIEF-GA-2011-298960) and partially by MINECO (Grant No. FPA2011-23596) and by LHCPhenonet (Grant No. PITN-GA-2010-264564). R. R. is supported by the *Landesgraduiertenförderung des Landes Baden-Württemberg*.

[1] S. Chatrchyan *et al.* (CMS Collaboration), Phys. Rev. D **89**, 012003 (2014).
[2] ATLAS collaboration, Report No. ATLAS-CONF-2013-079, 2013.
[3] T. Aaltonen *et al.* (CDF Collaboration, D0 Collaboration), Phys. Rev. Lett. **109**, 071804 (2012).
[4] O. Brein, A. Djouadi, and R. Harlander, Phys. Lett. B **579**, 149 (2004).
[5] G. Ferrera, M. Grazzini, and F. Tramontano, Phys. Rev. Lett. **107**, 152003 (2011).
[6] A. Denner, S. Dittmaier, S. Kallweit, and A. Muck, J. High Energy Phys. 03 (2012) 075.
[7] See e.g., J. Ellis, V. Sanz, and T. You, J. High Energy Phys. 07 (2014) 036, and references therein.
[8] S. Ji-Juan, M. Wen-Gan, Z. Ren-You, and G. Lei, Phys. Rev. D **81**, 114037 (2010).
[9] G. Luisoni, P. Nason, C. Oleari, and F. Tramontano, J. High Energy Phys. 10 (2013) 083.
[10] F. Campanario, C. Englert, and M. Spannowsky, Phys. Rev. D **82**, 054015 (2010).
[11] F. Campanario, C. Englert, and M. Spannowsky, Phys. Rev. D **83**, 074009 (2011).
[12] U. Baur, T. Han, and J. Ohnemus, Phys. Rev. D **48**, 5140 (1993).
[13] F. Campanario and S. Sapeta, Phys. Lett. B **718**, 100 (2012).
[14] F. Campanario, M. Rauch, and S. Sapeta, Nucl. Phys. **B879**, 65 (2014).
[15] K. Arnold *et al.*, Comput. Phys. Commun. **180**, 1661 (2009); arXiv:1107.4038; J. Baglio *et al.*, arXiv:1404.3940.
[16] J. Bellm, Diploma thesis, KIT, 2012, http://www.itp.kit.edu/prep/diploma/PSFiles/Diplom_Bellm.pdf.
[17] F. Campanario, C. Englert, S. Kallweit, M. Spannowsky, and D. Zeppenfeld, J. High Energy Phys. 07 (2010) 076.
[18] J. Ohnemus, Phys. Rev. D **44**, 3477 (1991).
[19] F. Campanario, C. Englert, M. Rauch, and D. Zeppenfeld, Phys. Lett. B **704**, 515 (2011).

[20] R. Roth, Diploma thesis, KIT, 2013, http://www.itp.kit.edu/prep/diploma/PSFiles/Diplom_Roth.pdf.
[21] K. Hagiwara and D. Zeppenfeld, Nucl. Phys. **B313**, 560 (1989).
[22] F. Campanario, J. High Energy Phys. 10 (2011) 070.
[23] T. Gleisberg, S. Höche, F. Krauss, M. Schönherr, S. Schumann, F. Siegert, and J. Winter, J. High Energy Phys. 02 (2009) 007.
[24] T. Gleisberg and S. Hoeche, J. High Energy Phys. 12 (2008) 039.
[25] W. Buchmuller and D. Wyler, Nucl. Phys. **B268**, 621 (1986).
[26] K. Hagiwara, S. Ishihara, R. Szalapski, and D. Zeppenfeld, Phys. Rev. D **48**, 2182 (1993).
[27] B. Grzadkowski, M. Iskrzynski, M. Misiak, and J. Rosiek, J. High Energy Phys. 10 (2010) 085.
[28] V. Hankele, G. Klamke, D. Zeppenfeld, and T. Figy, Phys. Rev. D **74**, 095001 (2006).
[29] T. Corbett, O. Eboli, J. Gonzalez-Fraile, and M. Gonzalez-Garcia, Phys. Rev. D **87**, 015022 (2013).
[30] E. Masso and V. Sanz, Phys. Rev. D **87**, 033001 (2013).
[31] VBFNLO utility to calculate form factors, version 1.3.0, https://www.itp.kit.edu/~vbfnloweb/wiki/doku.php?id=download:formfactor.
[32] H.-L. Lai, M. Guzzi, J. Huston, Z. Li, P. M. Nadolsky, J. Pumplin, and C.-P. Yuan, Phys. Rev. D **82**, 074024 (2010).
[33] M. Cacciari, G. P. Salam, and G. Soyez, J. High Energy Phys. 04 (2008) 063.
[34] I. W. Stewart and F. J. Tackmann, Phys. Rev. D **85**, 034011 (2012).
[35] A. Banfi, G. P. Salam, and G. Zanderighi, J. High Energy Phys. 06 (2012) 159.
[36] S. Gieseke, T. Kasprzik, and J. H. Kühn, Eur. Phys. J. C **74**, 2988 (2014).